Johann Radon Institute for
Computational and Applied Mathematics
Austrian Academy of Sciences (ÖAW)

Goal functional evaluations for phase-field fracture using PUM-based DWR mesh adaptivity

T. Wick

RICAM-Report 2015-47

Noname manuscript No.
(will be inserted by the editor)

Goal functional evaluations for phase-field fracture using PUM-based DWR mesh adaptivity

Thomas Wick

Received: date / Accepted: date

Abstract In this study, a posteriori error estimation plus goal-oriented mesh adaptivity are developed for phase-field fracture propagation. Goal functionals are treated with the dual weighted residual method (DWR) that is realized by a recently introduced novel localization technique based on a partition-of-unity (PU). This technique is straightforward to apply, as neither strong residuals nor jumps over element edges are required. Consequently, it facilitates the application of the DWR method to complex multiphysics problems such as fracture propagation. The algorithmic developments are substantiated with numerical tests.

Keywords finite elements, a priori error analysis, a posteriori error estimation, dual weighted residuals, adaptivity, phase-field fracture

Mathematics Subject Classification (2000) MSC 2010 65N30 · 65M60 · 49M15 · 35Q74

1 Introduction

The purpose of this article is on a posteriori error analysis accompanied with local mesh adaptivity for phase-field-based fracture propagation problems. Here, a novel variational localization technique within the dual-weighted residual (DWR) estimator is applied. Fracture propagation is presently one of the core topics in applied mathematics and engineering. Specifically, we are interested in variational formulations of quasi-static brittle fracture evolution problems that have been first formulated by Francfort & Marigo [27] accompanied with numerical findings presented in [19]. Here, discontinuities in the displacement field across the lower-dimensional crack surface are approximated by an auxiliary function φ. This function can be viewed as an indicator function, which introduces a diffusive transition zone between the broken and the unbroken material. This zone has a half bandwidth ε and is a model regularization parameter. Moreover, fracture evolutions satisfy a crack irreversibility constraint such that the resulting system can be characterized as a variational inequality. An important modification of [27] towards a thermodynamically-consistent *phase-field fracture* model has been accomplished by Miehe et al. [39,38]. The model in the present paper is build upon [39,38] and adds additionally a traction condition to treat pressurized fractures [40,41,57].

Despite the fact that phase-field fracture applications have been presented with impressive computational findings (see e.g., [39,16,36,51,3]) and likewise theoretical advancements based on energy minimization concepts treated with calculus of variations techniques [25,20]; systematic studies towards goal functional evaluations and a posteriori error estimation with local mesh adaptivity are rarely to find. An analysis of adaptive finite element approximations for fracture evolutions based on Ambrosio-Tortorelli approximations [4,5] has been carried out in [23,24]. Furthermore, mesh sensitivity studies have been addressed in [7,30].

However, special emphasize has often been on the crack path itself. First, this is of course of utter importance since the crack path describes the damaged zone

Thomas Wick
Johann Radon Institute for Computational and Applied Mathematics (RICAM),
Austrian Academy of Sciences,
Altenberger Str. 69, 4040 Linz, Austria
E-mail: thomas.wick@ricam.oeaw.ac.at

Fakultät für Mathematik, Lehrstuhl M17
Technische Universität München,
Boltzmannstr. 3, 85747 Garching bei München, Germany
E-mail: wick@ma.tum.de

of a material. Second, the model parameter ε is related to the discretization parameter h and must satisfy $\varepsilon > h$ in the crack region. Consequently, adaptive mesh refinement of a propagating fracture is tricky since the last condition might be violated. On the other hand, there are often situations in which other goal quantities (possibly far away from the crack path) such as stress values, solid deformations of the intact material or crack opening displacements require accurate evaluation.

As previously outlined, the main goal of this work is on a posteriori error analysis and spatial mesh adaptivity for which we apply the dual-weighted-residual (DWR) method. Here, a dual problem needs to be solved that provides sensitivity measures with respect to an error goal functional. The DWR technique goes back to Becker & Rannacher [10,11] and is based on pioneering work by Eriksson, Estep, Hansbo and Johnson [26]. Important further developments in the early stages have been accomplished in [1,43,42,28,21,9]. Among numerous applications (recent results in fluid-structure interaction, kinetic energy and isogeometric analysis can be found in [59,48,32,34]), we particularly list studies including variational inequalities [52,37,31] and emphasize the work of Rannacher & Suttmeier [44–47], Blum & Suttmeier [13,14], and Suttmeier [55,56] in elasticity/plasticity including quasi-stationary time evolutions and variational inequalities that have some common features with the present work. Moreover, we accentuate the study in [50] in which goal-oriented error estimation has also been applied to fracture problems but where the numerical discretization is carried out with extended finite elements (XFEM) rather than a phase-field model.

Most of these previous studies have in common that we either need the strong formulation [11] for the error localization or a special weak form with patched meshes [21]. In [49], a novel localization technique based on the weak form has been introduced that is straightforward to employ and easy to implement. In this localization, solution information about neighboring cells is gathered by employing a partition-of-unity (PU) (using a lowest-order finite element) leading to a nodal-based error indicator representation. In fact, working with a weakly-based error estimator is close to the early published work by Braack & Ern [21]. On the other hand, a PU for strongly localized DWR error estimation has been previously suggested by Kuzmin & Korotov [35].

The paper is organized as follows: In Section 2, we introduce notation and governing equations. Afterwards in Section 3, discretization and the solution algorithm for solving primal and dual problems are presented. Next in Section 4, the adaptive finite element framework using a posteriori error estimation and mesh adaptivity is formulated. Finally, in Section 5, we present several numerical examples that demonstrate the significance of our developments. The programming code is based on deal.II [8].

2 Notation and Modeling

In this section, we introduce basic notation and the weak form of the underlying equations. We denote the L^2 scalar product with $(\cdot,\cdot)$ as frequently used in the literature. In the following, let $\Omega \subset \mathbb{R}^2$, be a smooth, open, connected, and bounded set. We assume that the crack $\mathcal{C}$ is a 1-dimensional set, not necessarily connected, that is contained in Ω. The entire domain is defined as $B = \Omega \cup \overline{\mathcal{C}}$. We assume (possibly time-dependent non-homogeneous) Dirichlet boundaries conditions on the boundary $\partial\Omega_D$ and Neumann conditions on $\partial\Omega_N$; such that $\partial\Omega = \partial\Omega_D \cup \partial\Omega_N \cup \mathcal{C}$.

The unknown solution variables in phase-field-based fracture propagation are vector-valued displacements $u : B \to \mathbb{R}^2$ and a smoothed indicator phase-field function $\varphi : B \to [0,1]$. For $\varphi = 0$, we denote a crack region and $\varphi = 1$ is the unbroken material. The intermediate values constitute a so-called transition zone that is dependent on a regularization (or length-scale) parameter ε. The physics of the underlying problem ask to enforce a crack irreversibility condition (the crack can never heal) that is an inequality condition in time:

$$\partial_t \varphi \leq 0. \tag{1}$$

Consequently, fracture evolution problems lead to a variational inequality system and additionally, they are generically quasi-stationary or time-dependent. In the following we work with the incremental (i.e., time-discretized) formulation in which the continuous irreversibility constraint is approximated by

$$\varphi \leq \varphi^{old}.$$

Here, φ^{old} will later denote the previous time step solution and φ the current solution.

We are interested in the following system: Let $V := H_0^1(B)$ and

$$W_{in} := \{w \in H^1(B) |\, w \leq \varphi^{old} \leq 1 \text{ a.e. on } B\}$$

be the function spaces we work with here; and for later purposes we also need $W := H^1(B)$.

The system of equations applies to pressurized fractures and cracks in elasticity. In the former one, a non-homogeneous Neumann condition is applied to the crack surface; a detailed derivation and corresponding mathematical analysis can be found in [40,41]. The resulting Euler-Lagrange system reads:

Formulation 1 *Let $p \in H^1(B)$ be given. Find $(u, \varphi) \in \{u_D + V\} \times W$ such that*

$$\Big(\big((1-\kappa)\varphi^2 + \kappa\big)\,\sigma^+(u), e(w)\Big) + (\sigma^-(u), e(w)) + (\varphi^2 p, div\ w) = 0 \quad \forall w \in V, \tag{2}$$

and

$$(1-\kappa)(\varphi\,\sigma^+(u) : e(u), \psi-\varphi) + 2(\varphi\ p\ div\ u, \psi-\varphi) + G_c\Big(-\frac{1}{\varepsilon}(1-\varphi, \psi-\varphi) + \varepsilon(\nabla\varphi, \nabla(\psi-\varphi))\Big) \geq 0, \tag{3}$$

for all $\psi \in W_{in} \cap L^\infty(B)$.

This system does not explicitly contain time-derivatives. Rather, the time t might enter through time-dependent boundary conditions, e.g., $u_D = u_D(t) = g(t)$ on $\partial\Omega_D$ with a prescribed boundary function $g(t)$ of Dirichlet-type or time-dependent traction conditions (Neumann) or through time-dependent right hand side forces, e.g., a time-dependent pressure force $p := p(t)$.

In Formulation 1, κ is a positive regularization parameter for the elastic energy, with $\kappa = o(\varepsilon)$, and G_c is the critical energy release rate. Linear elasticity with the standard stress-strain relationship is defined as

$$\sigma := \sigma(u) = 2\mu e(u) + \lambda\ \mathrm{tr}(e(u))I.$$

Here, μ and λ are material parameters, $e(u) = \frac{1}{2}(\nabla u + \nabla u^T)$ is the strain tensor, and I the identity matrix. Furthermore, we use (see [38] and further comments made in [17]) the stress-splitting into tensile and compressive parts:

$$\sigma^+ = 2\mu e^+ + \lambda < \mathrm{tr}(e) > I,$$
$$\sigma^- = 2\mu(e - e^+) + \lambda\big(\mathrm{tr}(e) - < \mathrm{tr}(e) >\big)I,$$

and

$$e^+ = P\Lambda^+ P^T,$$

where $< \cdot >$ is the positive part of a function. Moreover, for $d = 2$,

$$\Lambda^+ := \Lambda^+(u) := \begin{pmatrix} < \lambda_1(u) > & 0 \\ 0 & < \lambda_2(u) > \end{pmatrix}.$$

where $\lambda_1(u)$ and $\lambda_2(u)$ are the eigenvalues of the strain tensor e, and $v_1(u)$ and $v_2(u)$ the corresponding (normalized) eigenvectors. Finally, the matrix P is defined as $P := P(u) := (v_1, v_2)$; namely, it consists of the column vectors $v_i, i = 1, 2$.

3 Primal and Dual Formulations and Basic Discretization

Our strategy is as follows: we first discretize in time and work with the resulting incremental formulations in order to formulate primal and dual problems. Finally, we briefly describe spatial discretization and the nonlinear iteration.

3.1 Temporal discretization

As already used in the definition of the space W_{in}, the irreversibility constraint (1) is discretized with a backward difference quotient such that

$$\frac{\varphi - \varphi^{n-1}}{\delta t} \leq 0,$$

where $\delta t = t^n - t^{n-1}$. Here, $\varphi^{n-1} := \varphi(t^{n-1})$ denotes the previous time step solution and $\varphi := \varphi^n := \varphi(t^n)$ the current solution. This constraint is later imposed with the help of simple penalization employing the penalization parameter $\gamma \in \mathbb{R}_+$ leading to the term

$$\gamma[\varphi - \varphi^{n-1}]^+$$

with $[x]^+ := max(0, x)$. It is well-known that the choice of γ is often delicate and heuristic while depending on material and discretization parameters; hints and ideas for elliptic problems are discussed, for example, in [33, 29, 58]. Better ways (however not adopted in this work) of imposing the above constraint for phase-field fracture are presented in [57, 30].

3.2 Primal and dual semi-linear forms

A well-known challenge in phase-field-based fracture formulations is related to the term

$$\big((1-\kappa)\varphi^2 + \kappa\big)\,\sigma^+(u),$$

that is on the energy level not convex in both solution variables u and φ simultaneously and requires sophisticated solution algorithms [20, 18, 23, 36] if one aims for finding a global minimum. However, the phase-field variable has no physical meaning and therefore, minimizing the total energy with respect to both solution variables u and φ remains questionable [2]. Combining these observations with several numerical studies that have been recently carried out in [30], we linearly extrapolate φ in time in the u-equation, in order to convexify the problem and to deal with a non-indefinite system. The extrapolated φ is denoted by $\tilde{\varphi}$ leading to

$$\big((1-\kappa)\tilde{\varphi}^2 + \kappa\big)\,\sigma^+(u).$$

On the one hand, this procedure is heuristic since in quasi-static fracture propagation, we cannot proof sufficient regularity in time; namely, the phase-field solution φ can have jumps in time. On the other hand, in [30], it has been numerically demonstrated that this procedure is very robust and has comparable accuracy for certain benchmarks as the other previously mentioned solution algorithms that have been suggested in the literature.

For our further purposes, we formulate a single semi-linear problem that reads: Find $U := \{u, \varphi\} \in \{u_D + V\} \times W$ such that

$$\begin{aligned} A(U)(\Psi) = &\Big(\big((1-\kappa)\tilde{\varphi}^2 + \kappa\big)\, \sigma^+(u), e(w)\Big) \\ &+ (\sigma^-(u), e(w)) + (\tilde{\varphi}^2 p, \operatorname{div} w) \\ &+ (1-\kappa)(\varphi\, \sigma^+(u) : e(u), \psi) \\ &+ 2(\varphi\, p \operatorname{div} u, \psi) \\ &+ G_c\Big(-\frac{1}{\varepsilon}(1-\varphi, \psi) + \varepsilon(\nabla\varphi, \nabla\psi)\Big) \\ &+ (\gamma[\varphi - \varphi^{n-1}]^+, \psi) = 0, \end{aligned} \tag{4}$$

for all $\Psi := \{w, \psi\} \in V \times W$.

Remark 1 Formulating a single semi-linear form of the coupled problem provides us with high accuracy of coupling conditions, but it is also necessary in the context of DWR error estimation for a consistent formulation of the dual problem and the entire error estimator.

The corresponding Jacobian is constructed by computing the directional derivative $A'(U)(\delta U, \Psi)$. Then, $\delta U := \{\delta u, \delta\varphi\} \in V \times W$ such that

$$\begin{aligned} &A'(U)(\delta U, \Psi) \\ &= \Big(\big((1-\kappa)\tilde{\varphi}^2 + \kappa\big)\, \sigma^+(\delta u), e(w)\Big) \\ &\quad + (\sigma^-(\delta u), e(w)) \\ &\quad + (1-\kappa)(\delta\varphi\sigma^+(u) : e(u) + 2\varphi\, \sigma^+(\delta u) : e(u), \psi) \\ &\quad + 2p(\delta\varphi \operatorname{div} u + \varphi \operatorname{div} \delta u, \psi) \\ &\quad + G_c\Big(\frac{1}{\varepsilon}(\delta\varphi, \psi) + \varepsilon(\nabla\delta\varphi, \nabla\psi)\Big) \\ &\quad + (\gamma\delta\varphi, \psi)_{A(\varphi)} = 0 \quad \forall \Psi := \{w, \psi\} \in V \times W, \end{aligned} \tag{5}$$

where

$$\mathcal{A}(\varphi) = \{x \in (0, L)^3 \,|\, \gamma(\varphi - \varphi^{n-1}) > 0\}.$$

In $\sigma^+(\delta u)$ and $\sigma^-(\delta u)$ we employ the derivative of e^+, which is given by

$$e^+(\delta u) = P(\delta u)\Lambda^+ P^T + P\Lambda^+(\delta u)P^T + P\Lambda^+ P^T(\delta u).$$

Formulation 2 (Primal form) *Find $U := \{u, \varphi\} \in \{u_D + V\} \times W$ such that*

$$A(U)(\Psi) = 0 \quad \forall \Psi := \{w, \psi\} \in V \times W, \tag{6}$$

where $A(U)(\Psi)$ is defined in (4).

For adjoint-based a posteriori error analysis (see Section 4), a dual problem needs to be solved in which an error functional $J : V \to \mathbb{R}$ enters as right hand side. Let $J : V \to \mathbb{R}$ be differentiable and let this functional describes errors; for example, point values and point stress values, line integrals or even global norms.

As usually, the dual form is obtained by switching test and ansatz functions in the linearized version of Formulation 2:

Formulation 3 (Dual form) *Find $Z := \{z^u, z^\varphi\} \in V \times W$ such that*

$$A'(U)(\Phi, Z) = J'(U)(\Phi) \quad \forall \Phi := \{\varphi^u, \varphi^\varphi\} \in V \times W. \tag{7}$$

Remark 2 The dual form is simply written down by formally changing the role of test and ansatz functions. The full form is omitted due to readability of the text. As usually done in practice, we just take the Jacobian of the (linearized) primal problem and transpose this matrix in order to obtain the dual form [11].

3.3 Spatial discretization and nonlinear iteration

All previous formulations are spatially discretized with a Galerkin finite element scheme, introducing H^1 conforming discrete spaces $V_h \subset V$ and $W_h \subset W$ consisting of bilinear functions Q_1^c on quadrilaterals. The discretization parameter is denoted by h. The spatial system of the primal problem is nonlinear due to the coupling of displacement and phase-field unknowns. The discretized version reads: Find $U_h \in \{u_D^h + V_h\} \times W_h$ such that

$$A(U_h)(\Psi) = 0 \quad \forall \Psi := \{w, \psi\} \in V_h \times W_h, \tag{8}$$

To solve this nonlinear problem, we employ a Newton scheme with simple backtracking.

For the iteration steps $m = 0, 1, 2, \ldots$, the Newton update $\delta U_h := \{\delta u_h, \delta\varphi_h\} \in V_h \times W_h$ is computed by solving:

$$\begin{aligned} A'(U_{h,m})(\delta U_h, \psi) &= -A(U_{h,m})(\Psi) \quad \forall \Psi \in V_h \times W_h, \\ U_{h,m+1} &= U_{h,m} + \omega \delta U_h, \end{aligned} \tag{9}$$

with a line search parameter $\omega \in (0, 1]$.

4 A Posteriori Error Estimation and Mesh Adaptivity

Our philosophy of goal-oriented a posteriori error estimation follows [46,47] who also considered quasi-stationary problems and variational inequalities. Rather than computing the dual problem backward in time, the time-evolving problems are split into a sequence of stationary problems (see again [45]). This means that time-dependent problems are discretized in time with a backward Euler scheme. In [46], Lemma 6.2, and Theorem 6.1, it has been shown that in the case of the quasi-stationary Prandtl-Reuss model, the error in each time/load step can accumulate at most linearly, which is the argument to neglect a full backward-time dual problem. Regarding the localization of the error indicators, we work with the weak form and a partition-of-unity (PU) as it has been recently proposed in [49]; thus avoiding integration by parts back into the strong form with higher order operators.

4.1 A partition-of-unity (PU) based variational localization of the DWR estimator

Let J be the goal (or target) functional. Relevant examples are stresses on faces Γ, point values or mean values

$$J(U) = \int_\Gamma \sigma \cdot n \, ds, \quad J(u) = u(x_0, y_0), \quad J(u) = \int_\Omega u \, dx.$$

Employing the dual problem, the a posteriori error estimator to such a functional reads [11]:

$$|J(U) - J(U_h)| \leq \sum_{T \in \mathbb{T}_h} \rho_T(U_h)\omega_T(Z),$$

with the local residuals $\rho_T(U_h)$ and sensitivity weights $\omega_T(Z)$. The above dual solution $Z \in V$ cannot be determined analytically but must be solved numerically as the primal problem, i.e, we search for $Z_h \in V_h$ by solving the discretized version of Formulation 3. However, it is well-known that Z_h must contain higher-order information either through local higher-order interpolation, computation on a finer mesh or higher polynomial degree [11].

This results in an approximate a posteriori error bound:

$$|J(U) - J(U_h)| \approx \eta = \sum_i^N \eta_i := \sum_{T \in \mathbb{T}_h} \rho_T(U_h)\tilde{\omega}_T(Z_h).$$

In the following, we use a recently introduced variational localization formulation [49] that only needs a partition-of-unity (PU), $\sum_i \chi_i \equiv 1$ which can be realized with lowest-order finite elements. The reason is that the local influence of neighboring cells is collected via the PU rather than integration by parts and face-term evaluation. The latter (well-known) classical technique becomes computationally expensive and intractable for multiphysics problems with many equations.

As PU, we consider the space of piece-wise bilinear elements $V_h^{(1)}$ (without restrictions on Dirichlet boundaries) with usual nodal basis $\{\chi_h^i,\ i = 1, \ldots, N\}$. The primal error estimator is then given by:

Proposition 1 *For the finite element approximation of Formulation 2, we have the a posteriori error estimate:*

$$\begin{aligned}
|J(U) - J(U_h)| &\leq \sum_i^N |\eta_i| \\
&= \sum_i^N \Big| \Big(-\big((1-\kappa)\tilde{\varphi}^2 - \kappa\big)\, \sigma^+(u), e(w) \Big) \\
&\quad - (\sigma^-(u), e(w)) - (\tilde{\varphi}^2 p, div\ w) \\
&\quad - (1-\kappa)(\varphi\, \sigma^+(u) : e(u), \psi) - 2(\varphi\, p\ div\ u, \psi) \\
&\quad - G_c \Big(-\frac{1}{\varepsilon}(1-\varphi, \psi) + \varepsilon(\nabla\varphi, \nabla\psi) \Big) \\
&\quad - (\gamma[\varphi - \varphi^{n-1}]^+, \psi) \Big|,
\end{aligned}$$

where the weighting functions are defined as

$$\begin{aligned}
w &:= (w_{2h}^{(2)} - z_h^u)\chi_h^i, \\
\psi &:= (\psi_{2h}^{(2)} - z_h^\varphi)\chi_h^i.
\end{aligned}$$

The first factors $w_{2h}^{(2)} - z_h^u$ and $\psi_{2h}^{(2)} - z_h^\varphi$ of the weights are standard [11]. Here, $w_{2h}^{(2)}$ is a higher-order finite element approximation (i.e., Q_2^c) of the dual solution z^u, respectively for $\psi_{2h}^{(2)}$ and z^φ. Of course, the dual problem is costly to solve. However in nonlinear problems, the (linearized) dual problem corresponds to one Newton solve, and is nonetheless cheaper than the related primal problem. The second function χ_h^i is the novel PU-function.

Proof From [11], we know the general error representation for the primal estimator:

$$\begin{aligned}
J(U) - J(U_h) = B(Z - i_h Z) - A(U_h)(Z - i_h Z) \\
+ R^2(U - U_h, Z - Z_h),
\end{aligned}$$

where i_h denotes an interpolation operator from the continuous spaces into the FE spaces. The functional

and semilinear forms are defined as

$$
\begin{aligned}
&B(Z - i_h Z) = -(\tilde{\varphi}^2 p, \mathrm{div}(z^u - i_h z^u)),\\
&A(U_h)(Z - i_h Z)\\
&\quad = \Big(\big((1-\kappa)\tilde{\varphi}^2 + \kappa\big)\ \sigma^+(u), e(z^u - i_h z^u) \Big)\\
&\qquad + (\sigma^-(u), e(z^u - i_h z^u))\\
&\qquad + (1-\kappa)(\varphi\ \sigma^+(u) : e(u), z^\varphi - i_h z^\varphi)\\
&\qquad + 2(\varphi\ p\ \mathrm{div}\ u, z^\varphi - i_h z^\varphi)\\
&\qquad + G_c \Big(-\frac{1}{\varepsilon}(1-\varphi,\psi) + \varepsilon(\nabla\varphi, \nabla(z^\varphi - i_h z^\varphi)) \Big)\\
&\qquad + (\gamma[\varphi - \varphi^{n-1}]^+, z^\varphi - i_h z^\varphi).
\end{aligned}
$$

Taking the absolute value yields:

$$
\begin{aligned}
|J(U) - J(U_h)| \leq\ & |B(Z - i_h Z) - A(U_h)(Z - i_h Z)|\\
&+ |R^2(U - U_h, Z - Z_h)|.
\end{aligned}
$$

Neglecting the remainder term and introducing the PU χ_h^i and summing over all degrees of freedom $i = 1, \ldots, N$ brings us to:

$$
\begin{aligned}
&|J(U) - J(U_h)|\\
&\quad \leq \sum_i^N |B((Z - i_h Z)\chi_h^i) - A(U_h)((Z - i_h Z)\chi_h^i)|.
\end{aligned}
$$

Inserting the definitions of $B(Z - i_h Z)$ and $A(U_h)(Z - i_h Z)$ and using the short notation $w := (w_{2h}^{(2)} - z_h^u)\chi_h^i$ and $\psi := (\psi_{2h}^{(2)} - z_h^\varphi)\chi_h^i$ yields the statement. Q.E.D.

We recall that the phase-field variable is, in the final end, an auxiliary variable without physical meaning. This goes hand in hand that the solution of the second PDE is only approximatively required; see also [2], p. 5013. Consequently an error estimator only based on the physical equation, namely for the displacements u, is given by:

Proposition 2 *For the first (i.e., the physical) equation of Formulation 2, discretized with finite elements, we have the a posteriori error estimate:*

$$
\begin{aligned}
&|J(U) - J(U_h)| \leq \sum_i^N |\eta_i|\\
&\quad = \sum_i^N \Big| \Big(-\big((1-\kappa)\tilde{\varphi}^2 - \kappa\big)\ \sigma^+(u), e(w) \Big)\\
&\qquad -(\sigma^-(u), e(w)) - (\tilde{\varphi}^2 p, div\ w) \Big|,
\end{aligned}
$$

where the weighting function is defined as

$$w := (w_{2h}^{(2)} - z_h^u)\chi_h^i.$$

In this formulation, the error estimator shrinks to elasticity with a fading elasticity coefficient $\big((1-\kappa)\tilde{\varphi}^2 + \kappa\big)$ *and a given right hand side* $\tilde{\varphi}^2 p$.

Proof Neglecting in Proposition 1 the phase-field related terms, yields immediately the assertion. Q.E.D.

Remark 3 (Evaluation of $\nabla(\chi\varphi)$ *for vector-valued problems)* Let χ the scalar-valued PU and let φ a vector-valued function. Then,

$$
\begin{aligned}
\nabla(\chi\varphi) &= \chi\nabla\varphi + \varphi \cdot \nabla\chi^T\\
&= \begin{pmatrix} \chi\partial_1\varphi_1, \chi\partial_2\varphi_1 \\ \chi\partial_1\varphi_2, \chi\partial_2\varphi_2 \end{pmatrix} + \begin{pmatrix} \varphi_1 \\ \varphi_2 \end{pmatrix} \cdot \Big(\partial_1\chi, \partial_2\chi \Big)\\
&= \begin{pmatrix} \chi\partial_1\varphi_1, \chi\partial_2\varphi_1 \\ \chi\partial_1\varphi_2, \chi\partial_2\varphi_2 \end{pmatrix} + \begin{pmatrix} \varphi_1\partial_1\chi, \varphi_1\partial_2\chi \\ \varphi_2\partial_1\chi, \varphi_2\partial_2\chi \end{pmatrix}.
\end{aligned}
$$

4.2 Mesh adaptation algorithms

Let an error tolerance TOL be given. The mesh adaptation is realized using extracted local error indicators from an a posteriori error estimate on the mesh $\mathbb{T}_h$.

$$|J(U) - J(U_h)| \leq \eta := \sum_{K\in\mathbb{T}_h} \sum_{i=1}^N |\eta_i| \quad \text{for all cells } K \in \mathbb{T}_h.$$

This information is used to adapt the mesh applying the following strategy:

1 Compute the primal solution U_h and the dual solution Z_h on the current mesh $\mathbb{T}_h$.
2 Determine the cell indicator η_i at each PU-nodal point.
3 Compute the sum of all indicators $\eta := \sum_{K\in\mathbb{T}_h} \eta_i$.
4 Check, if the stopping criterion is satisfied: $|J(U) - J(U_h)| \leq \eta \leq TOL$, then accept U_h within the tolerance TOL. Otherwise, proceed to the following step.

5a Mark all nodes i that belong to PU-nodal indicators η_i above the average $\frac{\alpha\eta}{N}$ (where N denotes the total number of nodes of the mesh $\mathbb{T}_h$ and $\alpha \approx 1$). All cells that touch this node will then be refined.

5b Alternatively: (coupling phase-field refinement with 5a) In addition to all cells marked in 5a, additional cells are marked for refinement in which the phase-field $\varphi < c$ with $c = 0.4$, for example.

5c Alternatively: the maximal mesh level might be fixed in 5a or 5b such that no overrefinement occurs in quasi-static or time-dependent problems.

Remark 4 (to strategy 5b) In phase-field based refinement, all cells are refined in which $\varphi < c$ (for example $c = 0.4$). This is important since the fracture propagates through the domain and too high parameter fluctuations (recall that ε is coupled to h via $h = o(\varepsilon)$ which can be realized by choosing, for instance, $\varepsilon = ch^l$,

$0 < l \leq 1$) should be avoided in the near fracture region. In coarse cells, ε remains large and influences the solution of the phase-field equation. A remedy has been presented in [30] in which a predictor-corrector scheme has been applied in order to ensure the 'correct' size of $\varepsilon > h$ at each time step of a propagating fracture with high mesh resolution. Since we deal with a quasi-static problem, we do not want to refine the mesh in each loading step in order to keep the total number of cells reasonable. We might fix the finest mesh level that should not be exceeded (strategy 5c). Another strategy by keeping the number of cells constant during time is explained in Remark 5.

Remark 5 Alternatively to 5a/5c: Order all nodes according to their size η_i. A fixed portion of nodes (i.e., their touching cells) with the smallest contributions to the total indicator η is marked to be deleted. In the second step, the nodes (i.e., cells) with the largest η_i are refined such that the desired number of cells N_{max} is approximately achieved. This strategy has been successfully applied for Prandtl-Reuss models in perfect plasticity [45,47]. We employ this technique in Example 5.3 in which the focus is on a goal functional error evaluation far away from the crack. Here, the near fracture condition $\varepsilon > h$ is violated on purpose while coarsening cells in that region.

4.3 Remarks to error estimation for phase-field fracture

So far in this section, we have formulated the error analysis with respect to the error $J(U) - J(U_h)$. However, the total error in phase-field fracture must be split into a model error and a discretization error; namely

$$J(U) - J(U_h) = J(U) - J(U_\varepsilon) + J(U_\varepsilon) - J(U_{\varepsilon,h}),$$

thus

$$|J(U) - J(U_h)| \leq \underbrace{|J(U) - J(U_\varepsilon)|}_{\text{Model err.}} + \underbrace{|J(U_\varepsilon) - J(U_{\varepsilon,h})|}_{\text{Discretization err.}}. \tag{10}$$

In fact, in this work we do only consider the DWR method for estimating the latter discretization error $|J(U_\varepsilon) - J(U_{\varepsilon,h})|$. Consequently, in Proposition 1 and 2 the continuous solution U should be replaced by the continuous-regularized solution U_ε and U_h by $U_{\varepsilon,h}$. A short numerical example that illustrates the influence of ε on the total error is provided in Section 5. However, systematic investigation and numerical analysis of the full error is to date a challenge and left for future research.

5 Numerical Examples

We discuss several numerical examples to substantiate our theoretical results and algorithmic developments.

5.1 A slit domain for scalar-valued displacements

This example considers the slit domain with displacement discontinuity (i.e., the crack) subject to a displacement field. In [6,15], a manufactured solution for the displacement field has been constructed. In our studies, the crack is presented by a phase-field function.

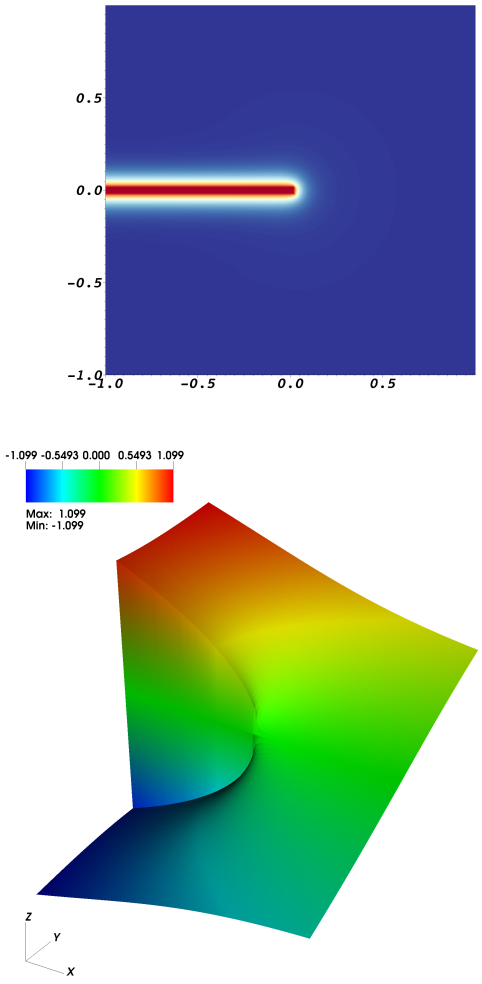

Fig. 1 Example 1: Crack, denoted in red color, (top) and 3D plot of the displacement field to show the discontinuity along the line $(x, 0)$ for $-1 \leq x \leq 0$.

Here, the continuous solution is given by $\varphi = 1$ in Ω and $\varphi = 0$ in $\mathcal{C}$. This allows us to study various scenarios such as $\varepsilon = h^l$ for different $l \in (0, 1]$. This choice is

motivated from the mathematical analysis of fracture models (i.e., free discontinuity problems) in which it is established that $h = o(\varepsilon)$ [22] (Appendix) with a full proof in [12].

For later purposes let us introduce the subdomain $\Omega_1 := \{x \in \Omega | \, |x| > 0.5\}$.

The model and material parameters are given as: $\kappa = 10^{-14}$, $G_c = \lambda^2_{G_c} \times \sqrt{\pi/2}$, $\lambda_{G_c} = 1.0$, $\mu = 1.0$. In this example, we set $p = 0$. For $\varepsilon = ch^l$, we study three test cases with

- Case 1: $c = 2.0$, $l = 1$,
- Case 2: $c = 0.5$, $l = 0.5$,
- Case 3: $c = 0.5$, $l = 0.25$.

The analytical solution on the slit domain $(-1, 1) \setminus \{(x, 0) | -1 \leq x \leq 0\}$ is given by [15]:

$$(\lambda r^{1/2} \sin \varphi/2; \{(x, 0) | -\infty \leq x \leq 0\})$$

where polar coordinates with $r^2 = x^2 + y^2$ are used. Employing the boundary function $g = \lambda \sin \varphi/2$ on $\partial\Omega$, we prescribe non-homogeneous Dirichlet conditions on all parts. Specifically, transforming g into Cartesian coordinates we have

$$x \leq 0 \text{ and } y \geq 0 : g(x, y) = \lambda/\sqrt{(2)} * \sqrt{\sqrt{x^2 + y^2} - x},$$
$$x \leq 0 \text{ and } y \leq 0 : g(x, y) = -\lambda/\sqrt{(2)} * \sqrt{\sqrt{x^2 + y^2} - x},$$
$$x \geq 0 \text{ and } y \geq 0 : g(x, y) = \lambda/\sqrt{(2)} * \sqrt{\sqrt{x^2 + y^2} - x},$$
$$x \geq 0 \text{ and } y \leq 0 : g(x, y) = -\lambda/\sqrt{(2)} * \sqrt{\sqrt{x^2 + y^2} - x}.$$

These conditions introduce a discontinuity on the boundary at $(-1, 0)$ and consequently a crack with displacement discontinuity as displayed in Figure 1.

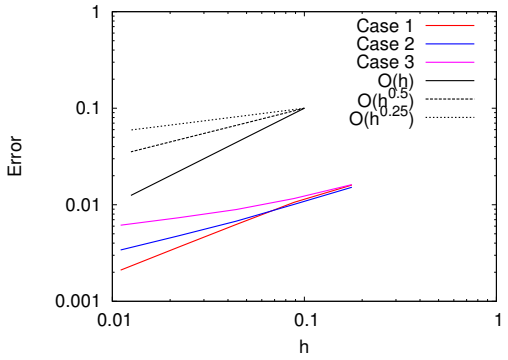

Fig. 2 Example 1a: Comparison of convergence rates of the total goal functional error $J(u) - J(u_{\varepsilon,h})$ for a displacement point value evaluation using uniform mesh refinement.

5.1.1 Influence of ε on goal functional evaluations

Motivated by Section 4.3, we compute a goal functional (here as an example a displacement point value in $u(0.75, -0.75)$) and consider the total error $J(u) - J(u_{\varepsilon,h})$. In order to reduce any other mesh-dependent effects, the mesh is uniformly refined. Analyzing our findings in Figure 2, we make the important observation that the maximal convergence order is $O(\varepsilon)$; namely in Case 2 $\varepsilon = 0.5$ and in Case 3 $\varepsilon = 0.25$. In Case 1, a slight reduced order $\varepsilon \approx 0.9$ is observed. This leads to the hypothesis that

$$|J(u) - J(u_{\varepsilon,h})| = O(\varepsilon).$$

In the following sections, it is shown that we however obtain higher order convergence while only considering the discretization error $J(u_\varepsilon) - J(u_{\varepsilon,h})$.

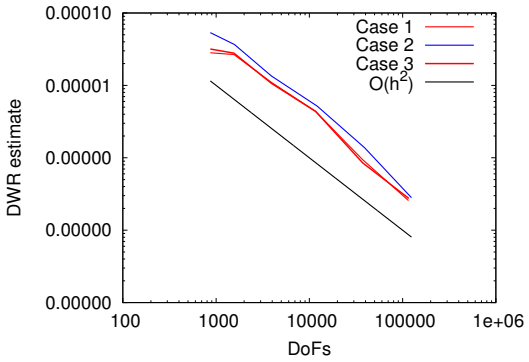

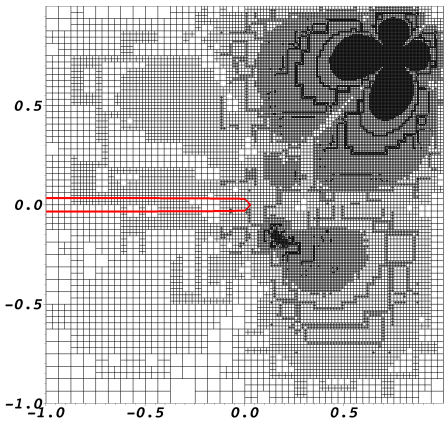

Fig. 3 Example 1b: DWR estimate (top) and locally refined mesh for the point functional evaluation. The crack contour for $\varphi = 0.05$ is displayed in red. We notice that the mesh is also refined at the crack tip since this introduces a geometrical singularity.

5.1.2 DWR error estimation

In this second test, the initial square domain is first four times globally refined; this mesh level is to be considered as the coarse mesh.

We study again different ε-h relationships and show that we obtain indeed optimal convergence rates with respect to h in Ω_1 while considering the error $J(u_\varepsilon) - J(u_{\varepsilon,h})$. This is demonstrated for two different goal functionals that are evaluated with the physical error estimator Proposition 2; namely

- A point functional in $u(0.75, -0.5)$ in Ω_1,
- The mean value $J(u) = \int_{\{(x,y)|y\leq -0.5\}} u\, dx$.

We compute again the Cases 1-3 in order to demonstrate that optimal order with respect to h can be achieved. Our findings are discussed in the Figures 3,4,5.

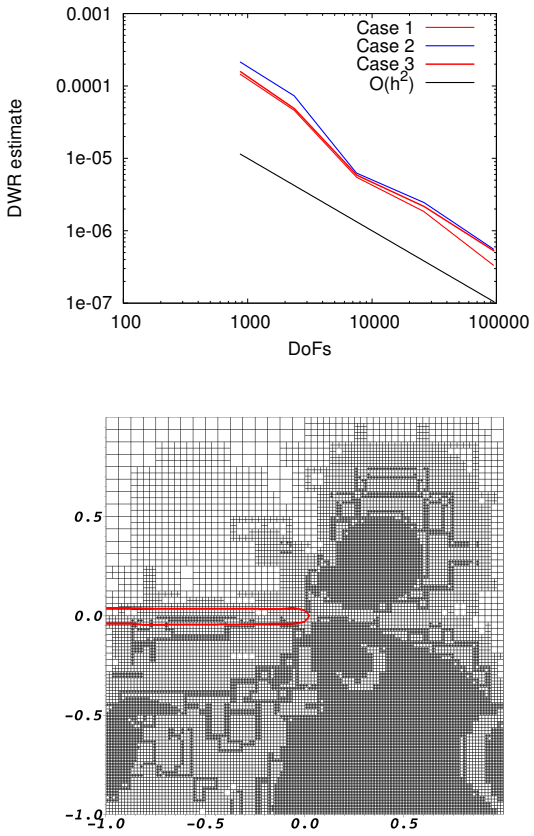

Fig. 4 Example 1b: DWR estimate (top) and locally refined mesh for the mean value functional evaluation. The crack contour for $\varphi = 0.05$ is displayed in red.

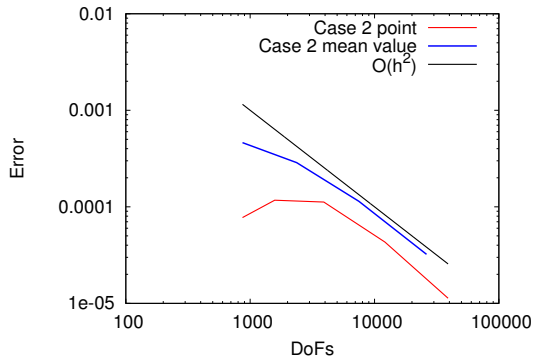

Fig. 5 Example 1b: Error plots for Case 2. We clearly identify that the order is not reduced when the error $J(u_\varepsilon) - J(u_{h,\varepsilon})$ is considered. This is due to the fact that we measure $J(u_{h,\varepsilon})$ with respect to $J(u_\varepsilon)$ rather than $J(u)$; namely, we study the second part of the triangle inequality (10).

5.2 A pressurized crack in elasticity

This test is a well-known benchmark in subsurface engineering considering pressurized fractures in elasticity or poroelasticity. The configuration is based on the theoretical calculations of [54,53] and leads to a stationary limit. Specifically, we study a 2D problem in which all data are given in dimensionless form; where a (constant) pressure $p = 10^{-3}$ is used to drive the deformation and crack width evolution. The configuration is the same as explained in [57]. Here, we deal with the following geometric data: $\Omega = (0,4)^2$ and a (prescribed) initial crack with length $l_0 = 0.4$ on $\Omega_C = (1.8-h, 2.2+h) \times (2-h, 2-h) \subset \Omega$. As before, the initial square domain is first four times globally refined; this mesh level is to be considered as the coarse mesh.

Let $\Gamma_{top} := \{(x,y)|y = 4\}$. As boundary conditions, we set the displacements to zero on $\partial\Omega$. In particular, the displacement field is now vector-valued. The model and material parameters are given as: $\kappa = 10^{-14}$, $G_c = 1.0$, $\nu_s = 0.2$, $E = 1.0$, $\gamma = 10$.

We study again different ε-h relationships and show that we obtain indeed optimal convergence rates in Ω_1 when considering the error $J(u_\varepsilon) - J(u_{\varepsilon,h})$. This is demonstrated for different goal functionals:

- Point error in $u(0.75, 0.75)$,
- stresses acting on Γ_{top}: $J(u) = \int_{\Gamma_{top}} \sigma \cdot n\, ds$ (on this boundary $\varphi \equiv 1$),
- the maximal crack opening displacement $J(U) = \int_\Gamma u \nabla\varphi\, ds$ on the middle line $\Gamma := \{(x,y)|\, x = 2\}$.

In addition, we compare for one test (see Figure 6) both error estimators defined in Proposition 1 and 2. In all other tests, we use Proposition 2. Our findings for the point functional and flux boundary are shown in

Figure 7 and 8. Here, our observations with respect to the convergence order confirm our findings of Example 2. Additionally, Figure 8 demonstrates good effectivity indices of the true error with respect to the DWR estimate.

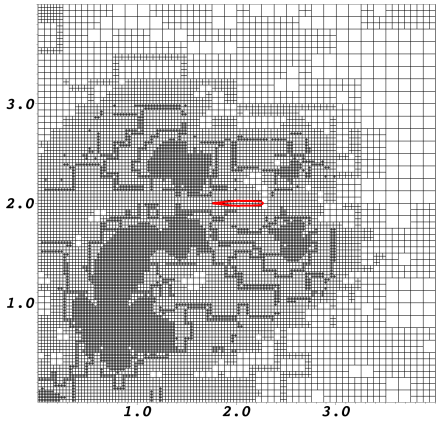

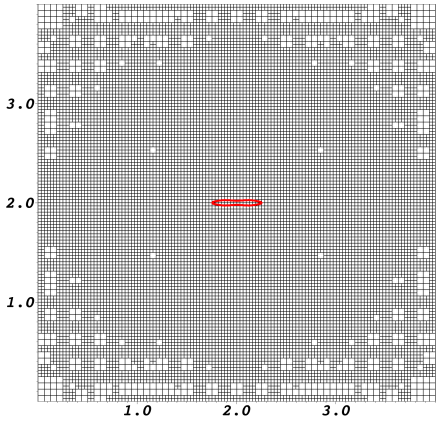

Fig. 6 Example 2: Locally refined meshes for the point value functional evaluation. The crack contour for $\varphi = 0.05$ is displayed in red. On top, the error estimator of Proposition 2 is used whereas the bottom figure displays the full estimator of Proposition 1. In the latter one, the error is overestimated and heavy overrefinement occurs.

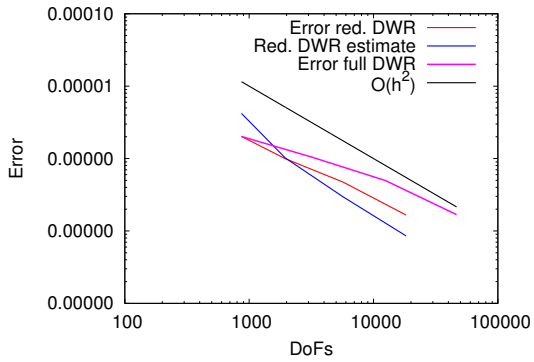

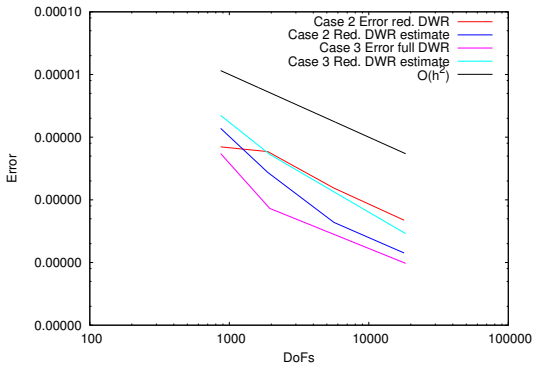

Fig. 7 Example 2: Point error evaluation for Case 1: comparison of the errors for the reduced error, and its DWR estimate (top). Although overrefinement occurs using the full estimator, the order of convergence is not affected. In the bottom figure, the error and DWR estimate for the reduced, physical, estimator are shown for the cases 2 and 3. As in Example 2, the convergence order is not affected by the choice of ε, Case 2 and 3, if $J(u_\varepsilon) - J(u_{\varepsilon,h})$ is taken to be the error of interest.

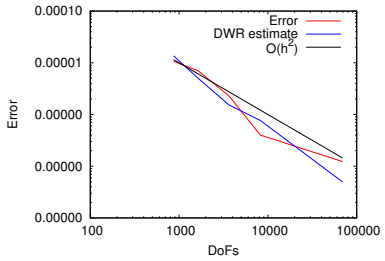

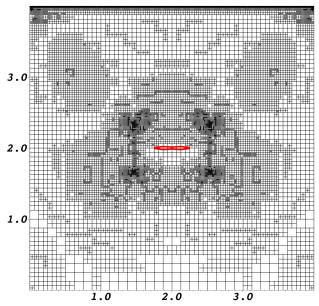

Fig. 8 Example 2: Locally refined mesh for the flux evaluation (Case 1) on the top boundary Γ_{top}. The crack contour for $\varphi = 0.05$ is displayed in red. Additionally, this example demonstrates good effectivity indices of the true error with respect to the DWR estimate.

To compute the maximal crack opening displacement, we work with the functional $J(U) = \int_\Gamma u \nabla\varphi \, ds$. The exact value can be determined with the help of [54] (Section 2.4). Our results are summarized in Table 1.

Table 1 Determining the maximal crack opening displacement.

Cells	$J(U) = \int_\Gamma u\nabla\varphi \, ds$
1516	7.32×10^{-4}
4408	5.56×10^{-4}
14416	4.69×10^{-4}
51916	4.44×10^{-4}
exact	3.84×10^{-4}

5.3 A propagating pressurized crack in elasticity

In this final example, we increase the pressure in time such that the crack starts propagating when the critical energy release rate is reached.

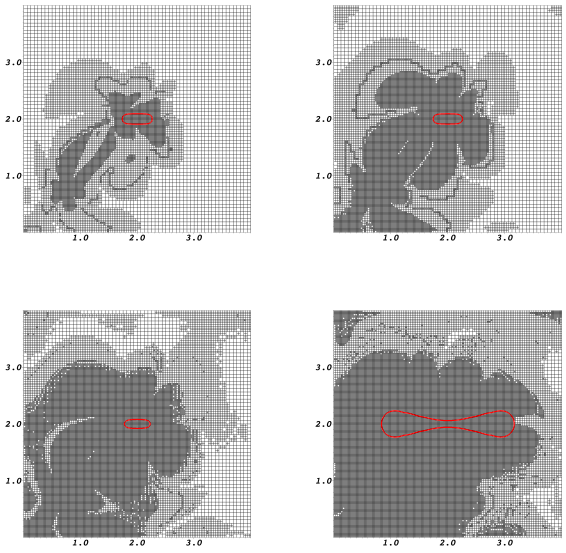

Fig. 9 Example 3: Adaptively refined meshes at times $T = 3, 4, 10, 20$ and crack contour ($\varphi = 0.4$) in red. Towards the end of the simulation, the mesh is mainly refined due to phase-field based refinement.

Here, the DWR-refinement (Proposition 2) is coupled with phase-field based refinement; namely strategy 5b (see also Remark 4). This technique is also compared to fixed fraction refinement in which only DWR refinement is used on patch and non-patched meshes. Here, we also allow for mesh coarsening of all cells that contribute to the smallest 10% of the total error. In addition, we keep the total number of cells fixed as explained in Remark 5.

The material and model parameters are the same as in the previous Example 5.2; except that ε is fixed at all times in a computation and initialized with $\varepsilon = h_{coarse}$. The coarse mesh is obtained by globally-refining the initial domain six times. In total 20 time steps with loading step size $\delta t = 1$ are computed.

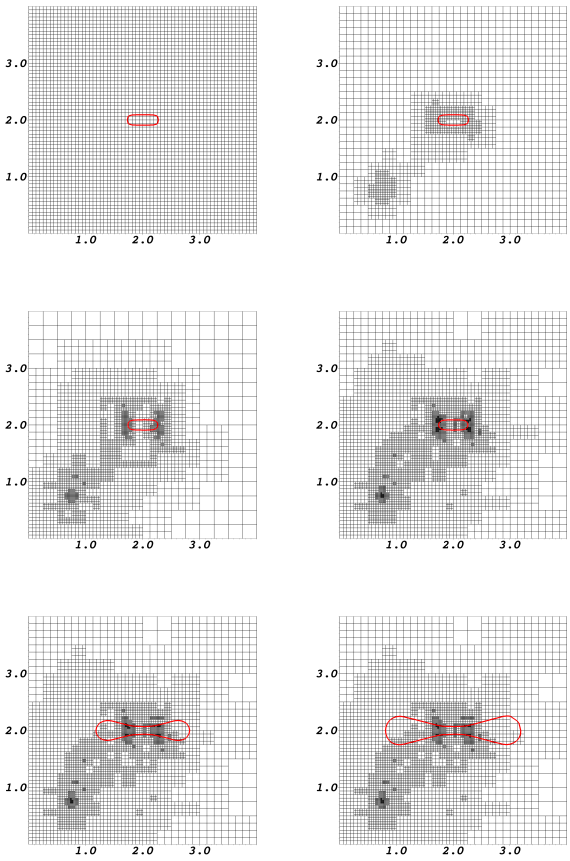

Fig. 10 Example 3: Adaptively refined meshes at times $T = 1, 2, 3, 4, 18, 20$ and crack contour ($\varphi = 0.4$) in red. Here, only patch-wise DWR refinement is employed such that the condition $\varepsilon > h$ is violated in the last steps. However, this violation has no significance influence on the goal functional evaluation. Moreover, this algorithm allows for coarsening as described in Remark 5.

The crack propagates due to a pressure that increases linearly in time:

$$p(t) = 0.1 + t \cdot 0.1,$$

where t denotes the current time.

In this example, we evaluate as goal functional the u_y displacement in $(0.75, 0.75)$ at the end time $T = 20$ (located in the left lower part of the domain). The

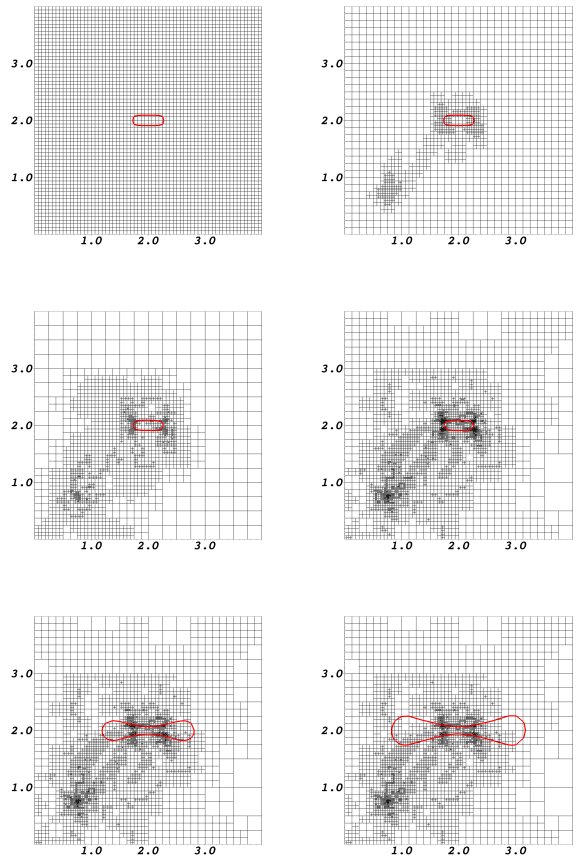

Fig. 11 Example 3: Adaptively refined meshes at times $T = 1, 2, 3, 4, 18, 20$ and crack contour ($\varphi = 0.4$) in red. Here, only non-patch DWR refinement is employed such that the condition $\varepsilon > h$ is violated in the last steps. However, this violation has no significance influence on the goal functional evaluation. Moreover, this algorithm allows for coarsening as described in Remark 5.

reference value computed on a fine mesh is

$$J(u_\varepsilon) = -0.581.$$

The u_y displacement field is displayed in Figure 12 to visualize the displacement discontinuity across the fracture. Locally adapted meshes are shown in Figure 9 for a sequence of different times. To achieve an approximate error $J(u_\varepsilon(T)) - J(u_{\varepsilon,h}(T)) \approx 10^{-2}$, we need around 18000 DoFs using DWR refinement and the double amount 40000 DoFs for DWR plus phase-field refinement; see Table 2. This result indicates that not always phase-field-based refinement is necessary in order to achieve good accuracy of goal functionals away from the fracture.

Finally, the evolution of the degrees of freedom versus time is provided in Figure 13.

Table 2 Goal functional error w.r.t. to different refinement strategies.

DoFs	Strategy	$J(u_\varepsilon(T)) - J(u_{\varepsilon,h}(T))$
39426	DWR plus phase-field	2.24×10^{-2}
18162	DWR non-patched	2.08×10^{-2}
18807	DWR patched	2.28×10^{-2}

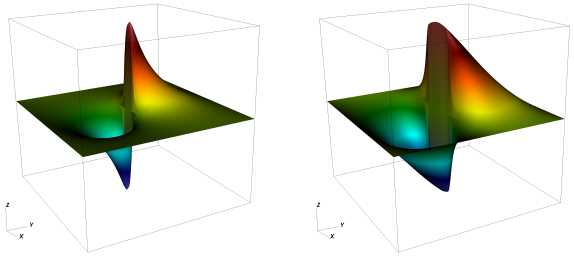

Fig. 12 Example 3: 3D plot of the u_y-displacement at $T = 3$ and $T = 20$ to illustrate the crack discontinuity in the middle of the domain.

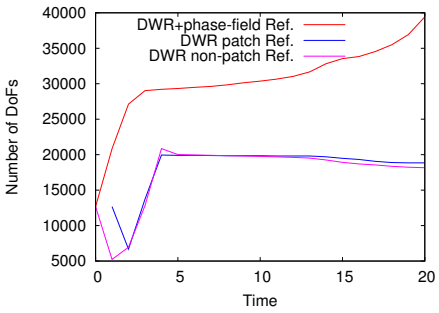

Fig. 13 Example 3: Development of degrees of freedom (DoFs) versus time for DWR plus phase-field refinement without mesh coarsening, DWR refinement using patched meshes, and DWR refinement with non-patched meshes. Using the first strategy, the number of degrees of freedom first increases due to the DWR estimator and later because of phase-field refinement due to the propagating fracture (see also Figure 9). For the two latter strategies the number of total degrees of freedom first drops due to mesh coarsening and later increases again. Here, a maximum number of 19 000 degrees of freedom is prescribed.

6 Conclusions

In this work, we developed goal-oriented a posteriori error estimation and mesh adaptivity for phase-field fracture propagation problems. Specifically, we applied a PU-based variational localization technique of the DWR method for quasi-stationary problems including a penalization term. This leads to a cost efficient solution algorithm for complex multiphysics problems such as fracture propagation. As seen in the algorithmic developments, the proposed method can be applied to pressurized fractures. Numerical tests substantiate our theory and adaptive schemes. In particular, we were able

to perform several convergence tests that provide further insight into the numerical mechanism of phase-field models for fractures. Here we emphasize that for the discretization error, we obtain expected convergence results. Furthermore, a brief inspection of model and discretization errors only yield reduced convergence that is of order from the regularization error. Finally, the last example demonstrates that phase-field-based refinement has less influence if a goal functional far away from the crack is considered. Future extensions of this work can be performed towards two directions: first, fluid-filled fractures in porous media in which additional equations are included and the ease of implementation of the PU-based DWR will pay off. Secondly, treatment of three-dimensional problems is envisaged in which mesh adaptivity helps enormously to reduce the computational cost.

References

1. M. Ainsworth and J. T. Oden. A posteriori error estimation in finite element analysis. *Computer Methods in Applied Mechanics and Engineering*, 142(1-2):1–88, 1997.
2. G. Allaire, F. Jouve, and N. V. Goethem. Damage and fracture evolution in brittle materials by shape optimization methods. *Journal of Computational Physics*, 230(12):5010 – 5044, 2011.
3. M. Ambati, T. Gerasimov, and L. De Lorenzis. A review on phase-field models of brittle fracture and a new fast hybrid formulation. *Computational Mechanics*, 55(2):383–405, 2015.
4. L. Ambrosio and V. Tortorelli. Approximation of functionals depending on jumps by elliptic functionals via γ-convergence. *Comm. Pure Appl. Math.*, 43:999–1036, 1990.
5. L. Ambrosio and V. Tortorelli. On the approximation of free discontinuity problems. *Boll. Un. Mat. Ital. B*, 6:105–123, 1992.
6. J. Andersson and H. Mikayelyan. The asymptotics of the curvature of the free discontinuity set near the cracktip for the minimizers of the Mumford-Shah functional in the plain. a revision. arXiv: 1205.5328v2, 2015.
7. M. Artina, M. Fornasier, S. Micheletti, and S. Perotto. Anisotropic mesh adaptation for crack detection in brittle materials. MOX Report 20/2014, 2014.
8. W. Bangerth, T. Heister, and G. Kanschat. *Differential Equations Analysis Library*, 2012.
9. W. Bangerth and R. Rannacher. *Adaptive Finite Element Methods for Differential Equations*. Birkhäuser, Lectures in Mathematics, ETH Zürich, 2003.
10. R. Becker and R. Rannacher. Weighted a posteriori error control in FE methods. In e. a. H. G. Bock, editor, *ENUMATH'97*. World Sci. Publ., Singapore, 1995.
11. R. Becker and R. Rannacher. *An optimal control approach to error control and mesh adaptation in finite element methods*, pages 1–102. Acta Numerica 2001, Cambridge University Press, a. iserles edition, 2001.
12. G. Belletini and A. Coscia. Discrete approximation of a free discontinuity problem. *Numer. Func. Anal. Optim.*, 15:201–224, 1994.
13. H. Blum and F.-T. Suttmeier. An adaptive finite element discretisation for a simplified signorini problem. 37(2):65–77, 1999.
14. H. Blum and F.-T. Suttmeier. Weighted error estimates for finite element solutions of variational inequalities. *Computing*, 65(2):119–134, 2000.
15. A. Bonnet and G. David. *Cracktip is a global Mumford-Shah minimizer*. Asterisque No. 274, 2001.
16. M. J. Borden, T. J. Hughes, C. M. Landis, and C. V. Verhoosel. A higher-order phase-field model for brittle fracture: Formulation and analysis within the isogeometric analysis framework. *Computer Methods in Applied Mechanics and Engineering*, 273(0):100 – 118, 2014.
17. M. J. Borden, C. V. Verhoosel, M. A. Scott, T. J. R. Hughes, and C. M. Landis. A phase-field description of dynamic brittle fracture. *Comput. Meth. Appl. Mech. Engrg.*, 217:77–95, 2012.
18. B. Bourdin. Numerical implementation of the variational formulation for quasi-static brittle fracture. *Interfaces and free boundaries*, 9:411–430, 2007.
19. B. Bourdin, G. Francfort, and J.-J. Marigo. Numerical experiments in revisited brittle fracture. *J. Mech. Phys. Solids*, 48(4):797–826, 2000.
20. B. Bourdin, G. Francfort, and J.-J. Marigo. The variational approach to fracture. *J. Elasticity*, 91(1–3):1–148, 2008.
21. M. Braack and A. Ern. A posteriori control of modeling errors and discretization errors. *Multiscale Model. Simul.*, 1(2):221–238, 2003.
22. A. Braides. *Approximation of free-discontinuity problems*. Springer Berlin Heidelberg, 1998.
23. S. Burke, C. Ortner, and E. Süli. An adaptive finite element approximation of a variational model of brittle fracture. *SIAM J. Numer. Anal.*, 48(3):980–1012, 2010.
24. S. Burke, C. Ortner, and E. Süli. An adaptive finite element approximation of a generalized Ambrosio-Tortorelli functional. *M3AS*, 23(9):1663–1697, 2013.
25. G. dal Maso, G. A. Francfort, and R. Toader. Quasistatic crack growth in nonlinear elasticity. *Arch. Ration. Mech. Anal.*, 176:165–225, 2005.
26. K. Eriksson, D. Estep, P. Hansbo, and C. Johnson. Introduction to adaptive methods for differential equations. In A. Iserles, editor, *Acta Numerica 1995*, pages 105–158. Cambridge University Press., 1995.
27. G. Francfort and J.-J. Marigo. Revisiting brittle fracture as an energy minimization problem. *J. Mech. Phys. Solids*, 46(8):1319–1342, 1998.
28. M. Giles and E. Süli. Adjoint methods for pdes: a posteriori error analysis and postprocessing by duality. *Acta Numerica 2002*, pages 145–236, 2002. A. Iserles, ed.
29. C. Groß mann and H.-G. Roos. *Numerische Behandlung partieller Differentialgleichungen*. Teubner-Studienbücher Mathematik ; Lehrbuch Mathematik. Teubner, Wiesbaden, 3., völlig überarb. und erw. aufl. edition, 2005.
30. T. Heister, M. F. Wheeler, and T. Wick. A primal-dual active set method and predictor-corrector mesh adaptivity for computing fracture propagation using a phase-field approach. *Comp. Meth. Appl. Mech. Engrg.*, 290(0):466 – 495, 2015.
31. M. Hintermüller, R. Hoppe, and C. Löbhard. Dual-weighted goal-oriented adaptive finite elements for optimal control of elliptic variational inequalities. *ESAIM: Control, Optimisation and Calculus of variations*, 20:524–546, 2014.
32. W. Hoitinga and E. van Brummelen. Goal-oriented adaptive methods for a boltzmann-type equation. volume 1333 of *AIP Conference Proceedings*, pages 81–86. American Institute of Physics, 2011.

33. N. Kikuchi and J. Oden. *Contact problems in elasticity*. Studies in Applied Mathematics. Society for Industrial and Applied Mathematics (SIAM), Philadelphia, PA, 1988.
34. G. Kuru, C. Verhoosel, K. van der Zee, and E. van Brummelen. Goal-adaptive isogeometric analysis with hierarchical splines. 270:270–292, 2014.
35. D. Kuzmin and S. Korotov. Goal-oriented a posteriori error estimates for transport problems. *Math. Comp. Sim.*, 80(8):1674 – 1683, 2010.
36. A. Mesgarnejad, B. Bourdin, and M. Khonsari. Validation simulations for the variational approach to fracture. *Computer Methods in Applied Mechanics and Engineering*, 290:420 – 437, 2015.
37. C. Meyer, A. Rademacher, and W. Wollner. Adaptive optimal control of the obstacle problem. *SIAM Journal on Scientific Computing*, 37(2):A918–A945, 2015.
38. C. Miehe, M. Hofacker, and F. Welschinger. A phase field model for rate-independent crack propagation: Robust algorithmic implementation based on operator splits. *Comput. Meth. Appl. Mech. Engrg.*, 199:2765–2778, 2010.
39. C. Miehe, F. Welschinger, and M. Hofacker. Thermodynamically consistent phase-field models of fracture: variational principles and multi-field fe implementations. *International Journal of Numerical Methods in Engineering*, 83:1273–1311, 2010.
40. A. Mikelić, M. Wheeler, and T. Wick. Phase-field modeling of a fluid-driven fracture in a poroelastic medium. accepted in Computational Geosciences, doi: 10.1007/s10596-015-9532-5, Sep 2013.
41. A. Mikelić, M. F. Wheeler, and T. Wick. A quasi-static phase-field approach to pressurized fractures. *Nonlinearity*, 28(5):1371–1399, 2015.
42. J. Oden and S. Prudhomme. On goal-oriented error estimation for elliptic problems: Application to the control of pointwise errors. *Comput. Methods Appl. Mech. Engrg.*, 176:313–331, 1999.
43. J. Peraire and A. Patera. Bounds for linear-functional outputs of coercive partial differential equations: local indicators and adaptive refinement. In P. Ladeveze and J. Oden, editors, *Advances in Adaptive Computational Methods in Mechanics*, pages 199–215. Elsevier, Amsterdam, 1998.
44. R. Rannacher and F.-T. Suttmeier. A feed-back approach to error control in finite element methods: application to linear elasticity. *Computational Mechanics*, 19(5):434–446, 1997.
45. R. Rannacher and F.-T. Suttmeier. A posteriori error control in finite element methods via duality techniques: Application to perfect plasticity. *Computational Mechanics*, 21(2):123–133, 1998.
46. R. Rannacher and F.-T. Suttmeier. A posteriori error estimation and mesh adaptation for finite element models in elasto-plasticity. *Computer Methods in Applied Mechanics and Engineering*, 176(1-4):333 – 361, 1999.
47. R. Rannacher and F.-T. Suttmeier. Error estimation and adaptive mesh design for FE models in elasto-plasticity. In E. Stein, editor, *Error-Controlled Adaptive FEMs in Solid Mechanics*. John Wiley, 2000.
48. T. Richter. Goal-oriented error estimation for fluid-structure interaction problems. *Comp. Methods Appl. Mech. Engrg.*, 223-224:38–42, 2012.
49. T. Richter and T. Wick. Variational localizations of the dual weighted residual estimator. *Journal of Computational and Applied Mathematics*, 279(0):192 – 208, 2015.
50. M. Rüter, T. Gerasimov, and E. Stein. Goal-oriented explicit residual-type error estimates in xfem. *Computational Mechanics*, 52(2):361–376, 2013.
51. A. Schlüter, A. Willenbücher, C. Kuhn, and R. Müller. Phase field approximation of dynamic brittle fracture. *Comput. Mech.*, 54:1141–1161, 2014.
52. A. Schr˙ Goal-oriented error control in adaptive mixed {FEM} for signorinis problem. *Computer Methods in Applied Mechanics and Engineering*, 200(14):345 – 355, 2011.
53. I. N. Sneddon. The distribution of stress in the neighbourhood of a crack in an elastic solid. *Proc. R Soc London A*, 187:229–260, 1946.
54. I. N. Sneddon and M. Lowengrub. *Crack problems in the classical theory of elasticity*. SIAM series in Applied Mathematics. John Wiley and Sons, Philadelphia, 1969.
55. F. Suttmeier. *Numerical solution of Variational Inequalities by Adaptive Finite Elements*. Vieweg+Teubne, 2008.
56. F.-T. Suttmeier. General approach for a posteriori error estimates for finite element solutions of variational inequalities. *Computational Mechanics*, 27(4):317–323, 2001.
57. M. Wheeler, T. Wick, and W. Wollner. An augmented-Lagangrian method for the phase-field approach for pressurized fractures. *Comp. Meth. Appl. Mech. Engrg.*, 271:69–85, 2014.
58. P. Wriggers. *Computational Contact Mechanics*. Springer, Berlin Heidelberg, 2006.
59. K. Zee, E. Brummelen, I. Akkerman, and R. Borst. Goal-oriented error estimation and adaptivity for fluid-structure interaction using exact linearized adjoints. *CMAME*, 200:2738–2757, 2011.